Available online at www.sciencedirect.com
ScienceDirect
International Journal of Heat and Mass Transfer 50 (2007) 4180–4194
International Journal of HEAT and MASS TRANSFER
www.elsevier.com/locate/ijhmt

Analysis of heat transfer and entropy generation for a thermally developing Brinkman–Brinkman forced convection problem in a rectangular duct with isoflux walls

K. Hooman [a,*], A. Haji-Sheikh [b]

[a] School of Engineering, The University of Queensland, Brisbane, Australia
[b] Department of Mechanical and Aerospace Engineering, The University of Texas at Arlington, 500 W. First Street, Arlington, TX 76019, USA

Received 10 January 2007; received in revised form 24 February 2007
Available online 3 May 2007

Abstract

Heat transfer and entropy generation analysis of the thermally developing forced convection in a porous-saturated duct of rectangular cross-section, with walls maintained at a constant and uniform heat flux, is investigated based on the Brinkman flow model. The classical Galerkin method is used to obtain the fully developed velocity distribution. To solve the thermal energy equation, with the effects of viscous dissipation being included, the extended weighted residuals method (EWRM) is applied. The local (three-dimensional) temperature field is solved by utilizing the Green's function solution based on the EWRM where symbolic algebra is being used for convenience in presentation. Following the computation of the temperature field, expressions are presented for the local Nusselt number and the bulk temperature as a function of the dimensionless longitudinal coordinate, the aspect ratio, the Darcy number, the viscosity ratio, and the Brinkman number. With the velocity and temperature field being determined, the second law (of thermodynamics) aspect of the problem is also investigated. Approximate closed form solutions are also presented for two limiting cases of *MDa* values. It is observed that decreasing the aspect ratio and *MDa* values increases the entropy generation rate.

Keywords: Porous media; Viscous dissipation; Extended weighted residuals method; Thermal development; Rectangular duct; Brinkman–Brinkman problem; Entropy generation

1. Introduction

Designed porous media, which are of current practical importance, are usually associated with such high permeability and porosity that the Darcy flow model is not applicable while the Brinkman flow model can predict hydraulics through such hyperporous media as noted by Nield and Bejan [1]. Flow through pores, in a microscopic scale, is inherently irreversible and a part of the mechanical power is dissipated to heat as a result of viscous dissipation. Consequently, this effect at the pore level is accounted for in macroscopic scale by retaining a viscous dissipation term in the thermal energy equation where the term is proportional to the volume-averaged velocity square as first noted by Ene and Sanchez-Palencia [2] for cases where the Darcy flow model is valid. On the other hand, as noted above, there are numerous cases of practical importance, where non-Darcy effects are significant and one should model the pore level dissipation in terms of appropriate properties (of fluid and solid matrix). However, for such cases one is left with two alternatives for the viscous dissipation function as proposed by Nield [3] and Al-Hadhrami et al. [4]. Recently, Breugem and Rees [5] have reported a volume averaging procedure to come up with a general model for viscous dissipation that seems to be applicable for a Brinkman–Brinkman problem. The term 'Brink-

* Corresponding author. Tel.: +61 (7) 33653668; fax: +61 (7) 33654799.
E-mail address: k.hooman@uq.edu.au (K. Hooman).

0017-9310/$ - see front matter © 2007 Elsevier Ltd. All rights reserved.
doi:10.1016/j.ijheatmasstransfer.2007.02.036

Nomenclature

A	area, m^2
$\mathbf{A}$	matrix
a, b	duct dimensions, see Fig. 1
a_{ij}	elements of matrix $\mathbf{A}$
$\mathbf{B}$	matrix
B_m	coefficients
Br	Brinkman number, $\mu_e U^2/(q_w a)$
b_{ij}	elements of matrix $\mathbf{B}$
$\bar{b}$	aspect ratio, $\bar{b} = b/a$
C	duct contour, m
c_p	specific heat, J/kg K
$\mathbf{D}$	matrix
Da	Darcy number, K/a^2
D_h	hydraulic diameter $4A/C$, m
d_{mj}	elements of matrix $\mathbf{D}$
$\mathbf{E}$	matrix with elements e_{ij}
e_{ij}	elements of matrix $\mathbf{E}$
F	pumping power to enthalpy change ratio, $F = P^*/(\rho c_p T^*)$
f_i, f_j	basis functions
G	Green's function
h	heat transfer coefficient, W/m^2 K
$\bar{h}$	average heat transfer coefficient, W/m^2 K
i, j	indices
K	permeability, m^2
k_e	effective thermal conductivity, W/m K
L	duct length, m
$\hat{L}$	dimensionless duct length, $L/(aPe)$
M	μ_e/μ
m, n	indices
$\dot{m}$	mass flow rate, kg/s
N	matrix dimension
N^*	dimensionless pressure drop, $N^* = P^*/(\mu U/K)$
N_s	dimensionless entropy generation rate, $\dot{S}_{gen}/(\dot{m}c_p)$
Nu	Nusselt number, ha/k_e
Nu_D	Nusselt number, hD_h/k_e
Nu^*	Nusselt number without viscous dissipation
$\mathbf{P}$	matrix having elements p_{mi}
P^*	$-\partial P^*/\partial x$, Pa/m
Pe	Péclet number, $\rho c_p a U/k_e$
P	pressure, Pa
p_{mi}	elements of matrix $\mathbf{P}$
q^*	dimensionless wall heat flux, $q^* = q_w a/(k_e T_i)$.
Re_D	Reynolds number, $\rho U D_h/\mu_e$
s	entropy, J/kg K
S	volumetric heat source, W/m^3
S^*	see Eq. (23b)
$\dot{S}_{gen}$	cross-sectional average of the entropy generation rate, W/K
T	temperature, K
T^*	dT_b/dx, K/m
T_i	temperature at $x = 0$, K
U	average velocity, m/s
$\overline{U}$	average value of $\bar{u}$
u	velocity, m/s
$\bar{u}$	dimensionless velocity, $\bar{u} = \mu u/(P^* a^2)$
x	axial coordinate, m
$\hat{x}$	$(x/a)/Pe$
y, z	coordinates, m
$\bar{y}, \bar{z}$	y/a and z/a

Greek symbols

Δ	vector with elements δ_i
δ_i	elements of vector Δ
η_j	basis functions, Eq. (2b)
θ	dimensionless temperature
λ_m	eigenvalues
μ	fluid viscosity, N s/m^2
μ_e	effective viscosity, N s/m^2
ξ	dimensionless coordinate
ρ	fluid density, kg/m^3
Φ	transformed temperature, Eq. (16)
ψ	eigenfunction
Ω	vectors with element ω_i
ω_i	elements of vector Ω

Subscripts

b	bulk
i	inlet condition
s	source effect
w	wall

man–Brinkman', proposed by Nield [6], refers to a problem involving a saturated porous medium in which the Brinkman momentum equation is used, and the thermal energy equation includes a viscous dissipation term involving a Brinkman number, which is the case here. It is also instructive to note that there are certain cases where one can neglect the effects of viscous dissipation as highlighted by Nield [6,7].

Regardless of the relative importance of the frictional heating compared to other heat transfer mechanisms in a system, there are some applications where one is willing to inspect the viscous dissipation effects. In an analysis of mantle flow, Bercovici [8] showed an example of the effects of viscous dissipation in self-lubricating systems. On the other hand, the recent work of Celata et al. [9] addresses an interesting application of viscous dissipation in measuring the fluid friction coefficient for flow in a micro-channel. In another notable study, Murakami and Mikic [10] have stated that even for flow of air, which has a relatively small viscosity compared to common liquids, say water, through

a micro-channel one should consider the effects of viscous dissipation when it comes to seek an optimum design feature. Moreover, when it comes to entropy generation minimization (EGM), which is a popular method of optimization, one should have a clear insight of the viscous dissipation as it emerges in the fluid friction term of entropy generation [11].

The groundbreaking work by Bejan [11] introduced the application of entropy generation due to heat and fluid flow as a powerful tool to optimize variety of configurations when analyzing engineering problems. Since entropy generation destroys the available work of a system, it makes good engineering sense to focus on entropy production due to heat transfer and fluid flow processes to understand the associated entropy generation mechanisms. The literature on the topic is rich for flow through unobstructed circular tubes or parallel plate channels. Similar work, mostly restricted to the fully developed region, extended the analysis to ducts of arbitrary cross-section [12,13], to name a few.

On the other hand, modeling entropy generation in porous media is comparatively harder than the clear fluid case partly due to the increased number of variables present in the governing equations. Another source of debate is the different available models for viscous dissipation, that lead to different fluid friction irreversibility (FFI) terms, as noted earlier. Moreover, the complexity of the problem becomes clearer when one observes that, numerical or theoretical, solutions addressing the second law analysis of forced convection in porous ducts are mostly restricted to circular tubes or parallel plate channels [14–17], where the simplicity of the geometry allows analytical solution of closed form. Thus the question naturally arises as to whether analytical solutions, addressing heat transfer and entropy generation, for more complicated cross-sections are possible.

The method of weighted residuals was exploited by Haji-Sheikh and Vafai [18] in their study of thermally developing convection in ducts of various shapes. In a subsequent study, Haji-Sheikh [19] has applied a Fourier series method to investigate fully developed forced convection in a duct of rectangular cross-section. Haji-Sheikh et al. [20–24] have investigated heat transfer characteristics of the thermal entrance region for flow through porous ducts of arbitrary cross-sections. Applying the Fourier series method, Hooman and Merrikh [25] have analytically investigated heat transfer and fluid flow in a rectangular duct occupied by a hyperporous medium.

A quick look at [18–25] shows that none of these articles reported the second law analysis. The work addressing this issue is limited to those applying the Darcy flow model in ducts of arbitrary cross-sections [26–28] with the exception of [29]. Hooman et al. [29] have reported heat transfer and entropy generation optimization in the fully developed region of a rectangular duct for three cases of **H1** boundary condition in the terminology of Shah and London [30]. This study treats the more general case of a thermally developing Brinkman–Brinkman problem in a duct of rectangular cross-section with walls held at a constant and uniform heat flux, i.e. the **H2** case [30]. To the authors' knowledge, not only there is no analytical solution available for the first law aspects of this problem but also the present assessment of entropy generation for a thermally developing Brinkman–Brinkman problem has not been reported elsewhere.

2. Analysis

2.1. Fluid flow analysis

For a passage with a constant but arbitrarily shaped cross-section, like the one depicted in Fig. 1, the Brinkman momentum equation reads

$$\mu_e\left(\frac{\partial^2 u}{\partial y^2}+\frac{\partial^2 u}{\partial z^2}\right)-\frac{\mu}{K}u-\frac{\partial p}{\partial x}=0. \tag{1}$$

Although an exact solution for fully developed velocity distribution is available, for convenience of symbolic manipulation, the classical Galerkin method is used for computation of velocity. It begins by setting

$$u(y,z)=\sum_{j=1}^{N}\delta_j\eta_j(y,z), \tag{2a}$$

where

$$\eta_j=(a^2-y^2)(b^2-z^2)y^{2(m_j-1)}z^{2(n_j-1)} \tag{2b}$$

and δ_j coefficients are the constants to be determined. Next, the substitution of $u(y,z)$ from Eq. (2a) in momentum

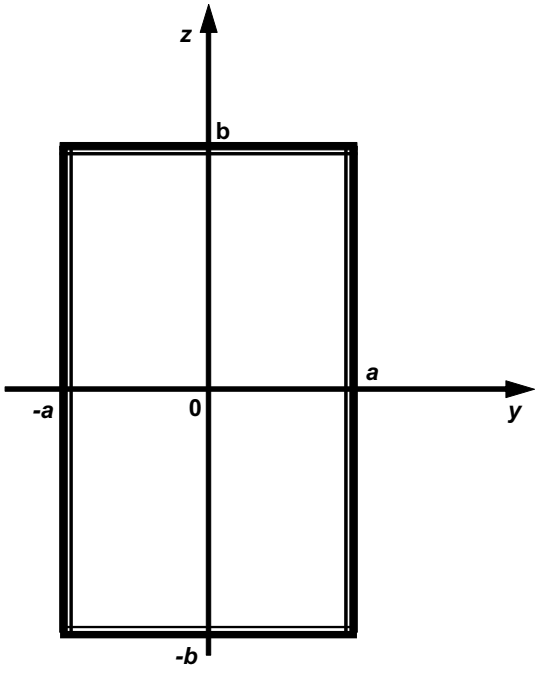

Fig. 1. A schematic of a rectangular passage with coordinates.

equation, Eq. (1), and following the procedure in [31] leads to

$$\mathbf{E}\cdot\mathbf{\Delta}=\Omega, \tag{3a}$$

with matrix $\mathbf{E}$ and vector Ω having elements

$$e_{ij}=\int_A[\mu_e\eta_i(\mathbf{y},z)\nabla^2\eta_j(\mathbf{y},z)-\mu\eta_j/K]\mathrm{d}A, \tag{3b}$$

and

$$\omega_i=\left(\frac{\partial p}{\partial x}\right)\int_A\eta_i(y,z)\mathrm{d}A, \tag{3c}$$

where A is the cross-sectional area of the duct. Therefore, the unknown coefficients are members of the vector $\Delta=\{\delta_1,\delta_2,\ldots,\delta_N\}$ obtainable from $\mathbf{\Delta}=\mathbf{E}^{-1}\cdot\Omega$. Once the local velocity distribution is determined, the mean velocity can be obtained as

$$U=\frac{1}{A}\int_A u\,\mathrm{d}A, \tag{4a}$$

and the normalized velocity is

$$\hat{u}=\frac{u}{U}. \tag{4b}$$

2.2. Heat transfer analysis

2.2.1. Governing thermal energy equation

Under the local thermal equilibrium condition, the energy equation, in its general form, for hydrodynamically fully developed and incompressible flow is

$$(\rho c_p)_f u\frac{\partial T}{\partial x}=\frac{\partial}{\partial x}\left(k_e\frac{\partial T}{\partial x}\right)+\frac{\partial}{\partial y}\left(k_e\frac{\partial T}{\partial y}\right)+\frac{\partial}{\partial z}\left(k_e\frac{\partial T}{\partial z}\right)+S(x,y,z), \tag{5}$$

where $S(x,y,z)$ includes the contribution of frictional heating and parameters $(\rho c_p)_f$ and k_e are the fluid thermal

Table 1
The parameter S^*, for different b/a and MDa values, for determination of $\Phi_{2,b}=S^*\cdot\hat{x}$

MDa	$b/a=1$	$b/a=2$	$b/a=4$	$b/a=10$
0.0001	10202.9	10151.6	10126.3	10111.5
0.001	1066.07	1049.09	1040.81	1035.90
0.01	123.042	116.772	113.871	112.199
0.1	20.1833	16.9485	15.6872	15.0167
1	8.48230	5.70568	4.83563	4.42943
10	7.25128	4.50748	3.68970	3.32534
∞	7.11354	4.37289	3.56109	3.20179

Table 2a
The difference between the dimensionless wall temperature and bulk temperature due to the wall effect and frictional heating contribution when $b/a=1$

$\hat{x}$	$MDa=\infty$		$MDa=1$		$MDa=1/10$	
	$\theta_{1,w}-\theta_{1,b}$	$\Phi_{2,w}-\Phi_{2,b}$	$\theta_{1,w}-\theta_{1,b}$	$\Phi_{2,w}-\Phi_{2,b}$	$\theta_{1,w}-\theta_{1,b}$	$\Phi_{2,w}-\Phi_{2,b}$
0.0005	0.0949	0.044	0.0928	0.046	0.0816	0.061
0.0006	0.1012	0.049	0.0990	0.051	0.0870	0.068
0.0008	0.1119	0.058	0.1095	0.061	0.0963	0.080
0.001	0.1211	0.067	0.1184	0.070	0.1043	0.090
0.002	0.1545	0.102	0.1512	0.106	0.1333	0.132
0.003	0.1783	0.131	0.1745	0.134	0.1540	0.163
0.004	0.1971	0.155	0.1930	0.159	0.1705	0.189
0.005	0.2130	0.176	0.2086	0.180	0.1844	0.212
0.006	0.2269	0.196	0.2223	0.200	0.1966	0.231
0.008	0.2505	0.231	0.2454	0.235	0.2174	0.265
0.01	0.2703	0.262	0.2649	0.265	0.2348	0.294
0.02	0.3402	0.381	0.3337	0.382	0.2969	0.397
0.03	0.3868	0.469	0.3796	0.468	0.3386	0.467
0.04	0.4219	0.540	0.4143	0.536	0.3703	0.519
0.05	0.4499	0.600	0.4420	0.592	0.3958	0.561
0.06	0.4731	0.650	0.4649	0.641	0.4169	0.596
0.08	0.5095	0.733	0.5010	0.719	0.4502	0.651
0.1	0.5369	0.798	0.5280	0.780	0.4753	0.692
0.2	0.608	0.974	0.5984	0.947	0.5406	0.802
0.3	0.633	1.039	0.6231	1.007	0.5632	0.840
0.4	0.6422	1.063	0.6322	1.029	0.5714	0.854
0.5	0.6457	1.072	0.6356	1.038	0.5744	0.859
0.6	0.6470	1.075	0.6369	1.041	0.5755	0.861
0.8	0.6477	1.077	0.6376	1.042	0.5760	0.862
1	0.6478	1.077	0.6377	1.043	0.5761	0.862
2	0.6478	1.077	0.6377	1.043	0.5761	0.862
3	0.6478	1.077	0.6377	1.043	0.5761	0.862
4	0.6478	1.077	0.6377	1.043	0.5761	0.862
5	0.6478	1.077	0.6377	1.043	0.5761	0.862

capacity and the equivalent thermal conductivity, respectively. When the contribution of axial conduction is negligible, Eq. (5) reduces to

$$\frac{\partial}{\partial y}\left(k_{\mathrm{e}}\frac{\partial T}{\partial y}\right)+\frac{\partial}{\partial z}\left(k_{\mathrm{e}}\frac{\partial T}{\partial z}\right)+S(y,z;x)=(\rho c_{\mathrm{p}})_{\mathrm{f}}u\frac{\partial T}{\partial x}. \tag{6}$$

The solution for Eq. (6) with a prescribed wall heat flux and in the presence of frictional heating is possible as

$$T(y,z;x)=\sum_{m=1}^{N}B_m\Psi_m(y,z)\mathrm{e}^{-\lambda_m^2 x}, \tag{7a}$$

where

$$\Psi_m=\sum_{j=1}^{N}d_{mj}f_j(y,z). \tag{7b}$$

The following set of basis functions satisfies the homogeneous boundary condition of the second kind along the walls,

$$f_j=(1+(m_j-1)(1-\bar{y}^2))(1+(n_j-1)(1-\bar{z}^2/\bar{b}^2))\bar{y}^{2(m_j-1)}\bar{z}^{2(n_j-1)}, \tag{8}$$

for all combinations of $m_j=1,2,\ldots$ and $n_j=1,2,\ldots$. The eigenvalues are λ_m^2 and the coefficients d_{mj} are the members of eigenvectors $\mathbf{d_m}$; they are obtainable from the relation

$$(\mathbf{A}+\lambda_m^2\mathbf{B})\cdot\mathbf{d_m}=0, \tag{9}$$

where the elements of the matrices **A** and **B** are

$$a_{ij}=-\int_A k_{\mathrm{e}}\nabla f_i(y,z)\cdot\nabla f_j(y,z)\mathrm{d}A \tag{10a}$$

$$b_{ij}=\int_A \rho c_{\mathrm{p}}u(y,z)f_i(y,z)f_j(y,z)\mathrm{d}A. \tag{10b}$$

After determination of λ_m^2 and d_{mj}, the appropriate mathematical steps in [32] provide the general solution. The eigenvectors $\mathbf{d_m}$ will constitute the rows of a matrix **D**. When the boundary conditions are homogeneous and the thermophysical properties are constant, the Green's function solution is

$$T(y,z;x)=\frac{1}{\rho c_{\mathrm{p}}}\int_{\xi=0}^{x}\mathrm{d}\xi\int_A GS(y',z';\xi)\mathrm{d}A'+\int_A u(y',z')G(y,z,x|y',z',0)T(y',z';0)\mathrm{d}A', \tag{11}$$

wherein the Green's function is

$$G(y,z,x|y',z',\xi)=\sum_{m=1}^{N}\left[\sum_{i=1}^{N}p_{mi}f_i(y',z')\right]\Psi_m(y,z)\mathrm{e}^{-\lambda_m^2(x-\xi)}. \tag{12}$$

Table 2b
The difference between the dimensionless wall temperature and bulk temperature due to the wall effect and frictional heating contribution when $b/a=1$

$\hat{x}$	$MDa=1/100$		$MDa=1/1000$		$MDa=1/10{,}000$	
	$\theta_{1,\mathrm{w}}-\theta_{1,\mathrm{b}}$	$\Phi_{2,\mathrm{w}}-\Phi_{2,\mathrm{b}}$	$\theta_{1,\mathrm{w}}-\theta_{1,\mathrm{b}}$	$\Phi_{2,\mathrm{w}}-\Phi_{2,\mathrm{b}}$	$\theta_{1,\mathrm{w}}-\theta_{1,\mathrm{b}}$	$\Phi_{2,\mathrm{w}}-\Phi_{2,\mathrm{b}}$
0.0005	0.0609	0.132	0.0441	0.132	0.0441	0.274
0.0006	0.0647	0.143	0.0471	0.143	0.0471	0.292
0.0008	0.0714	0.162	0.0521	0.162	0.0521	0.313
0.001	0.0773	0.177	0.0564	0.177	0.0564	0.325
0.002	0.0991	0.234	0.0727	0.234	0.0727	0.345
0.003	0.1146	0.272	0.0847	0.272	0.0847	0.354
0.004	0.1271	0.300	0.0944	0.300	0.0944	0.360
0.005	0.1376	0.322	0.1028	0.322	0.1028	0.364
0.006	0.1469	0.341	0.1102	0.341	0.1102	0.367
0.008	0.1627	0.370	0.1229	0.370	0.1229	0.371
0.01	0.1761	0.392	0.1337	0.392	0.1337	0.374
0.02	0.2240	0.459	0.1733	0.459	0.1733	0.381
0.03	0.2565	0.494	0.2009	0.494	0.2009	0.383
0.04	0.2814	0.517	0.2223	0.517	0.2223	0.385
0.05	0.3016	0.533	0.2398	0.533	0.2398	0.386
0.06	0.3185	0.546	0.2545	0.546	0.2545	0.386
0.08	0.3453	0.564	0.2783	0.564	0.2783	0.387
0.1	0.3658	0.577	0.2966	0.577	0.2966	0.388
0.2	0.4197	0.608	0.3461	0.608	0.3461	0.389
0.3	0.4383	0.618	0.3638	0.618	0.3638	0.389
0.4	0.4448	0.622	0.3701	0.622	0.3701	0.389
0.5	0.4471	0.623	0.3725	0.623	0.3725	0.389
0.6	0.4479	0.624	0.3733	0.624	0.3733	0.389
0.8	0.4483	0.624	0.3737	0.624	0.3737	0.389
1	0.4484	0.624	0.3738	0.624	0.3738	0.389
2	0.4484	0.624	0.3738	0.624	0.3738	0.389
3	0.4484	0.624	0.3738	0.624	0.3738	0.389
4	0.4484	0.624	0.3738	0.624	0.3738	0.389
5	0.4484	0.624	0.3738	0.624	0.3738	0.389

The parameters p_{mi} in Eq. (12) are members of the matrix $\mathbf{P} = [(\mathbf{D}\cdot\mathbf{B})^{\mathrm{T}}]^{-1}$ (see Chapter 10 of [32] for more details). In dimensionless space, the temperature solution in rectangular passages takes the following form

$$T(\bar{y},\bar{z};\hat{x}) = \frac{1}{\rho c_{\mathrm{p}}}\int_{\xi=0}^{\hat{x}} \mathrm{d}\xi \int_{\bar{z}=0}^{\bar{b}}\int_{\bar{y}=0}^{1} G(\bar{y},\bar{z},\hat{x}|\bar{y}',\bar{z}',\xi)S(\bar{y}',\bar{z}')\mathrm{d}\bar{y}'\,\mathrm{d}\bar{z}' + \int_{\bar{z}=0}^{\bar{b}}\int_{\bar{y}=0}^{1} u(\bar{y}',\bar{z}')G(\bar{y},\bar{z},\hat{x}|\bar{y}',\bar{z}',0)T(y,z;0)\mathrm{d}\bar{y}'\,\mathrm{d}\bar{z}' \tag{13}$$

wherein the Green's function is

$$G(\bar{y},\bar{z},\hat{x}|\bar{y}',\bar{z}',\xi) = \sum_{m=1}^{N}\left[\sum_{i=1}^{N} p_{mi} f_i(\bar{y}',\bar{z}')\right]\Psi_m(y,z)\mathrm{e}^{-\lambda_m^2(\hat{x}-\xi)} \tag{14}$$

and

$$S(\bar{y}',\bar{z}') = \frac{\mu_{\mathrm{e}}U^2}{q_{\mathrm{w}}^a}\left[\frac{\hat{u}^2}{MDa} + \left(\frac{\partial\hat{u}}{\partial\bar{y}'}\right)^2 + \left(\frac{\partial\hat{u}}{\partial\bar{z}'}\right)^2\right]. \tag{15}$$

The next task is the computation of the temperature in the entrance region of rectangular passages with locally constant wall heat flux q_{w}. For the EWRM, the boundary conditions should be homogeneous. Therefore, the following temperature transformation, in the dimensionless form, is being used for insertion into the energy equation,

$$\theta(\bar{y},\bar{z};\hat{x}) = \frac{T(y,z;x)-T_{\mathrm{i}}}{q_{\mathrm{w}}a/k_{\mathrm{e}}} = \Phi(\bar{y},\bar{z};\hat{x}) + \frac{\bar{y}^2}{2} + \frac{\bar{z}^2}{2\bar{b}}, \tag{16}$$

where $q_{\mathrm{w}} = k_{\mathrm{e}}\partial T/\partial y|_{y=a} = k_{\mathrm{e}}\partial T/\partial z|_{z=b}$ is the input heat flux. After substituting for T from this transformation in Eq. (16), the function $\Phi(\bar{y},\bar{z};\hat{x})$ must satisfy the following equation

$$\frac{\partial^2\Phi}{\partial\bar{y}^2} + \frac{\partial^2\Phi}{\partial\bar{z}^2} + \frac{\mu_{\mathrm{e}}U^2}{q_{\mathrm{w}}a}\left[\frac{\hat{u}^2}{MDa} + \left(\frac{\partial\hat{u}}{\partial\bar{y}}\right)^2 + \left(\frac{\partial\hat{u}}{\partial\bar{z}}\right)^2\right] + \frac{\bar{b}+1}{\bar{b}} = \left(\frac{u}{U}\right)\frac{\partial\Phi}{\partial\hat{x}}. \tag{17}$$

Now, the new function $\Phi(\bar{y},\bar{z};\hat{x})$ satisfies the boundary conditions $\partial\Phi/\partial\bar{y}|_{\bar{y}=0} = \partial\Phi/\partial\bar{y}|_{\bar{y}=1} = 0, \partial\Phi/\partial\bar{z}|_{\bar{z}=0} = \partial\Phi/\partial\bar{z}|_{\bar{z}=\bar{b}} = 0$ and the entrance condition $\Phi(\bar{y},\bar{z};0) = -(\bar{y}^2+\bar{z}^2/\bar{b})/2$.

The equation for $\Phi(\bar{y},\bar{z};\hat{x})$ contains a heat source expression that results from viscous dissipation in a porous medium modeled by the Brinkman equation, in the form recommended in [4]. Also it contains an additional source term that emerged following the transformation. This suggests a development of two separate solutions; first, $\Phi_1(\bar{y},\bar{z};\hat{x})$ by neglecting the contribution of viscous dissipation and using the quantity $(\bar{b}+1)/\bar{b}$ as the only

Table 3a
The difference between the dimensionless wall temperature and bulk temperature due to the wall effect and frictional heating contribution when $b/a = 2$

$\hat{x}$	$MDa=\infty$		$MDa=1$		$MDa=1/10$	
	$\theta_{1,\mathrm{w}}-\theta_{1,\mathrm{b}}$	$\Phi_{2,\mathrm{w}}-\Phi_{2,\mathrm{b}}$	$\theta_{1,\mathrm{w}}-\theta_{1,\mathrm{b}}$	$\Phi_{2,\mathrm{w}}-\Phi_{2,\mathrm{b}}$	$\theta_{1,\mathrm{w}}-\theta_{1,\mathrm{b}}$	$\Phi_{2,\mathrm{w}}-\Phi_{2,\mathrm{b}}$
0.0005	0.0995	0.034	0.0964	0.037	0.0819	0.054
0.0006	0.1059	0.038	0.1027	0.041	0.0875	0.060
0.0008	0.1170	0.045	0.1134	0.049	0.0968	0.070
0.001	0.1264	0.052	0.1224	0.056	0.1046	0.080
0.002	0.1611	0.080	0.1558	0.085	0.1329	0.116
0.003	0.1855	0.103	0.1795	0.108	0.1532	0.143
0.004	0.2051	0.122	0.1985	0.128	0.1695	0.165
0.005	0.2218	0.139	0.2145	0.145	0.1834	0.185
0.006	0.2363	0.155	0.2286	0.161	0.1955	0.202
0.008	0.2610	0.182	0.2526	0.189	0.2161	0.231
0.01	0.2819	0.207	0.2728	0.214	0.2335	0.256
0.02	0.3564	0.303	0.3452	0.309	0.2963	0.344
0.03	0.4071	0.374	0.3946	0.378	0.3392	0.402
0.04	0.4463	0.432	0.4327	0.433	0.3724	0.446
0.05	0.4783	0.480	0.4638	0.479	0.3996	0.481
0.06	0.5054	0.522	0.4902	0.519	0.4227	0.510
0.08	0.5495	0.591	0.5331	0.584	0.4602	0.555
0.1	0.5845	0.646	0.5671	0.635	0.4898	0.590
0.2	0.6922	0.808	0.6713	0.784	0.5792	0.683
0.3	0.7496	0.883	0.7264	0.852	0.6248	0.722
0.4	0.7860	0.925	0.7610	0.888	0.6527	0.740
0.5	0.8110	0.951	0.7848	0.911	0.6717	0.751
0.6	0.8291	0.968	0.8020	0.926	0.6855	0.758
0.8	0.8524	0.990	0.8243	0.945	0.7033	0.766
1	0.8656	1.003	0.8369	0.955	0.7136	0.771
2	0.8822	1.018	0.8529	0.969	0.7270	0.777
3	0.8832	1.019	0.8539	0.969	0.7279	0.778
4	0.8832	1.019	0.8539	0.970	0.7280	0.778
5	0.8832	1.019	0.8539	0.970	0.7280	0.778

contribution for the wall effect. The second solution $\Phi_2(\bar{y},\bar{z};\hat{x})$ is to use $S(y',z',\xi)$ in the Green's function solution for the frictional contribution and this makes $\Phi(\bar{y},\bar{z};\hat{x}) = \Phi_1(\bar{y},\bar{z};\hat{x}) + Br\Phi_2(\bar{y},\bar{z};\hat{x})$ with $Br = \mu_e U^2/(q_w a)$. Splitting Eq. (13) into two equations; the first contribution is

$$\Phi_1(\bar{y},\bar{z};\hat{x}) = \int_{\bar{\xi}=0}^{\hat{x}} \mathrm{d}\xi \int_{\bar{z}=0}^{\bar{b}} \int_{\bar{y}=0}^{1} G(\bar{y},\bar{z},\hat{x}|\bar{y}',\bar{z}',\xi)\left(\frac{1+\bar{b}}{\bar{b}}\right)\mathrm{d}\bar{y}'\,\mathrm{d}\bar{z}' - \int_{\bar{z}=0}^{\bar{b}} \int_{\bar{y}=0}^{1} u(\bar{y}',\bar{z}')G(\bar{y},\bar{z},\hat{x}|\bar{y}',\bar{z}',0)\left(\frac{\bar{y}^2}{2}+\frac{\bar{z}^2}{2\bar{b}}\right)\mathrm{d}\bar{y}'\,\mathrm{d}\bar{z}' \tag{18}$$

and the second one is

$$\Phi_2(\bar{y},\bar{z};\hat{x}) = \int_{\bar{\xi}=0}^{\hat{x}} \mathrm{d}\xi \int_{\bar{z}=0}^{\bar{b}} \int_{\bar{y}=0}^{1} G(\bar{y},\bar{z},\hat{x}|\bar{y}',\bar{z}',\xi)\left[\frac{\hat{u}^2}{MDa} + \left(\frac{\partial\hat{u}}{\partial\bar{y}'}\right)^2 + \left(\frac{\partial\hat{u}}{\partial\bar{z}'}\right)^2\right]\mathrm{d}\bar{y}'\,\mathrm{d}\bar{z}' \tag{19}$$

wherein the Green's function is defined by Eq. (14).

This form of the Green's function contains the basis functions $f_i(\bar{y}',\bar{z}')$, eigenfunctions $\Psi_m(\bar{y},\bar{z})$, parameters P_{mi}, and eigenvalues λ_m^2. The second contribution, following substitution for the Green's function, attains a standard form,

$$\Phi_2(\bar{y},\bar{z};\hat{x}) = \sum_{m=1}^{N} A_m \Psi_m(\bar{y},\bar{z})\frac{1-\mathrm{e}^{-\lambda_m^2\hat{x}}}{\lambda_m^2}, \tag{20}$$

where

$$A_m = \sum_{i=1}^{N} p_{mi}\int_{\bar{z}=0}^{\bar{b}}\int_{\bar{y}=0}^{1}\left[\frac{\hat{u}^2}{MDa}+\left(\frac{\partial\hat{u}}{\partial\bar{y}'}\right)^2+\left(\frac{\partial\hat{u}}{\partial\bar{z}'}\right)^2\right]f_i(\bar{y}',\bar{z}')\mathrm{d}\bar{y}'\,\mathrm{d}\bar{z}'. \tag{21}$$

It is to be noted that as $\hat{x}$ becomes large, the solution for Φ_2 approaches that for the quasi thermally fully developed solution $\Phi_{2,FD}$. Therefore, the solution using equation

$$\Phi_2(\bar{y},\bar{z};\hat{x}) = \Phi_{2,FD} - \sum_{m=1}^{N} A_m \Psi_m(\bar{y},\bar{z})\frac{\mathrm{e}^{-\lambda_m^2\hat{x}}}{\lambda_m^2} \tag{22}$$

exhibits better convergence characteristics. The solution for $\Phi_{2,FD}$ uses the Poisson's equation

$$\frac{\partial^2\Phi_{2,FD}}{\partial\bar{y}^2}+\frac{\partial^2\Phi_{2,FD}}{\partial\bar{z}^2}+Br\left[\frac{\hat{u}^2}{MDa}+\left(\frac{\partial\hat{u}}{\partial\bar{y}}\right)^2+\left(\frac{\partial\hat{u}}{\partial\bar{z}}\right)^2\right]-S^*\hat{u}=0, \tag{23a}$$

where

$$S^* = \int_{\bar{z}=0}^{\bar{b}}\int_{\bar{y}=0}^{1}\left[\frac{\hat{u}^2}{MDa}+\left(\frac{\partial\hat{u}}{\partial\bar{y}'}\right)^2+\left(\frac{\partial\hat{u}}{\partial\bar{z}'}\right)^2\right]\mathrm{d}\bar{y}'\,\mathrm{d}\bar{z}' \tag{23b}$$

Table 3b
The difference between the dimensionless wall temperature and bulk temperature due to the wall effect and frictional heating contribution when $b/a = 2$

$\hat{x}$	$MDa = 1/100$		$MDa = 1/1000$		$MDa = 1/10{,}000$	
	$\theta_{1,w}-\theta_{1,b}$	$\Phi_{2,w}-\Phi_{2,b}$	$\theta_{1,w}-\theta_{1,b}$	$\Phi_{2,w}-\Phi_{2,b}$	$\theta_{1,w}-\theta_{1,b}$	$\Phi_{2,w}-\Phi_{2,b}$
0.0005	0.0591	0.123	0.0423	0.252	0.0334	0.285
0.0006	0.0633	0.134	0.0454	0.269	0.0361	0.296
0.0008	0.0706	0.154	0.0508	0.295	0.0407	0.312
0.001	0.0767	0.169	0.0554	0.314	0.0446	0.324
0.002	0.0983	0.223	0.0726	0.366	0.0595	0.352
0.003	0.1133	0.258	0.0848	0.391	0.0703	0.362
0.004	0.1254	0.285	0.0945	0.408	0.0792	0.367
0.005	0.1358	0.305	0.1028	0.420	0.0868	0.370
0.006	0.1450	0.323	0.1101	0.429	0.0937	0.372
0.008	0.1607	0.350	0.1229	0.442	0.1057	0.376
0.01	0.1740	0.370	0.1339	0.452	0.1161	0.378
0.02	0.2222	0.432	0.1747	0.475	0.1550	0.382
0.03	0.2556	0.464	0.2036	0.486	0.1829	0.383
0.04	0.2816	0.485	0.2264	0.492	0.2050	0.384
0.05	0.3031	0.500	0.2454	0.496	0.2235	0.384
0.06	0.3214	0.511	0.2617	0.500	0.2394	0.383
0.08	0.3513	0.528	0.2887	0.504	0.2657	0.383
0.1	0.3751	0.539	0.3103	0.507	0.2869	0.382
0.2	0.4472	0.568	0.3767	0.515	0.3522	0.380
0.3	0.4833	0.578	0.4103	0.517	0.3853	0.378
0.4	0.5050	0.583	0.4304	0.519	0.4051	0.377
0.5	0.5196	0.586	0.4438	0.519	0.4182	0.376
0.6	0.5301	0.587	0.4535	0.520	0.4277	0.375
0.8	0.5440	0.589	0.4663	0.520	0.4402	0.374
1	0.5522	0.590	0.4739	0.521	0.4476	0.374
2	0.5633	0.592	0.4845	0.521	0.4582	0.373
3	0.5642	0.592	0.4854	0.521	0.459	0.373
4	0.5642	0.592	0.4854	0.521	0.4591	0.373
5	0.5642	0.592	0.4854	0.521	0.4591	0.373

and it is obtainable by different methods. Since symbolic algebra is being used, it is determined by the classical Galerkin method [31]. Alternatively, a known $\Phi_{2,FD}$ solution leads to an initial value problem similar to that used to obtain Φ_1 instead of the second term on the right side of Eq. (22).

Once the functions $\Phi_1(\bar{y},\bar{z};\hat{x})$ and $\Phi_2(\bar{y},\bar{z};\hat{x})$ are known, the temperature solution $\theta(\bar{y},\bar{z};\hat{x})$ is available. Accordingly, for convenience of this presentation, the two contributions of the dimensionless temperature $\theta(\bar{y},\bar{z};\hat{x}) = \theta_1(\bar{y},\bar{z};\hat{x}) + \theta_2(\bar{y},\bar{z};\hat{x})$ are presented separately; that is,

$$\theta_1(\bar{y},\bar{z};\hat{x}) = \frac{\bar{y}^2}{2} + \frac{\bar{z}^2}{2\bar{b}} + \Phi_1(\bar{y},\bar{z};\hat{x}) \tag{24}$$

and

$$\theta_2(\bar{y},\bar{z};\hat{x}) = Br\Phi_2(\bar{y},\bar{z};\hat{x}). \tag{25}$$

Therefore, for $i = 1$ or 2, the following equation provides the mean wall temperature for each contribution,

$$\theta_{i,w}(\hat{x}) = \frac{1}{1+\bar{b}}\left[\int_{\bar{y}=0}^{1}\theta_i(\bar{y},\bar{b};\hat{x})\mathrm{d}\bar{y} + \int_{\bar{z}=0}^{\bar{b}}\theta_i(1,\bar{z};\hat{x})\mathrm{d}\bar{z}\right] \tag{26}$$

2.3. Second law analysis

Cross-sectional average of the entropy generation rate $\dot{S}_{gen}$ can be found as [12]

$$\mathrm{d}\dot{S}_{gen} = \dot{m}\,\mathrm{d}s - \frac{\delta Q}{T_w}. \tag{27}$$

Noting that the longitudinal pressure gradient is constant, $-\frac{\mathrm{d}P}{\mathrm{d}x} = P^*$, with $\mathrm{d}s = c_p\frac{\mathrm{d}T_b}{T_b} - \frac{\mathrm{d}P}{\rho T_b}$ and $\delta Q = q_w C\,\mathrm{d}x$, and after some algebraic manipulations one has

$$\frac{\mathrm{d}\dot{S}_{gen}}{\dot{m}c_p} = \frac{\mathrm{d}T_b}{\mathrm{d}x}\frac{\mathrm{d}x}{T_b} - \frac{P^*\,\mathrm{d}x}{\rho c_p T_b} - \frac{q_w C\,\mathrm{d}x}{\dot{m}c_p T_w}. \tag{28}$$

On the other hand, the first law of thermodynamics for an element reads

$$\frac{\mathrm{d}T_b}{\mathrm{d}x} = \frac{4q_w(1+\bar{b})a^3 + \mu_e U^2 S * A}{\dot{m}c_p a^2} = T^*, \tag{29}$$

where T^* is a constant (longitudinal bulk temperature gradient). Solving for the bulk temperature, one has

$$T_b = T^* x + T_i. \tag{30}$$

Making use of the above equation in the entropy production formula, Eq. (28), one concludes

Table 4a
The difference between the dimensionless wall temperature and bulk temperature due to the wall effect and frictional heating contribution when $b/a = 4$

$\hat{x}$	$MDa = \infty$		$MDa = 1$		$MDa = 1/10$	
	$\theta_{1,w} - \theta_{1,b}$	$\Phi_{2,w} - \Phi_{2,b}$	$\theta_{1,w} - \theta_{1,b}$	$\Phi_{2,w} - \Phi_{2,b}$	$\theta_{1,w} - \theta_{1,b}$	$\Phi_{2,w} - \Phi_{2,b}$
0.0005	0.0936	0.033	0.0902	0.035	0.0767	0.050
0.0006	0.1002	0.037	0.0965	0.040	0.0819	0.056
0.0008	0.1114	0.044	0.1073	0.047	0.0910	0.067
0.001	0.1209	0.051	0.1165	0.055	0.0988	0.076
0.002	0.1551	0.079	0.1497	0.083	0.1276	0.113
0.003	0.1786	0.101	0.1726	0.106	0.1478	0.140
0.004	0.1970	0.119	0.1904	0.125	0.1636	0.162
0.005	0.2125	0.136	0.2054	0.141	0.1767	0.180
0.006	0.2260	0.151	0.2184	0.157	0.1881	0.197
0.008	0.2490	0.178	0.2407	0.184	0.2074	0.225
0.01	0.2684	0.202	0.2594	0.208	0.2236	0.248
0.02	0.3377	0.293	0.3266	0.298	0.2819	0.333
0.03	0.3849	0.360	0.3723	0.364	0.3218	0.389
0.04	0.4214	0.414	0.4075	0.416	0.3525	0.430
0.05	0.4512	0.459	0.4364	0.459	0.3777	0.463
0.06	0.4765	0.497	0.4608	0.495	0.3990	0.490
0.08	0.5177	0.558	0.5006	0.553	0.4336	0.533
0.1	0.5505	0.606	0.5321	0.599	0.4609	0.565
0.2	0.6530	0.737	0.6295	0.722	0.5429	0.648
0.3	0.7109	0.790	0.6834	0.770	0.5853	0.678
0.4	0.7513	0.815	0.7205	0.792	0.6130	0.691
0.5	0.7830	0.829	0.7493	0.804	0.6341	0.697
0.6	0.8096	0.839	0.7734	0.813	0.6514	0.701
0.8	0.8528	0.853	0.8125	0.824	0.6793	0.706
1	0.8873	0.863	0.8437	0.832	0.7016	0.710
2	0.9921	0.890	0.9385	0.853	0.7702	0.718
3	1.0416	0.901	0.9836	0.863	0.8035	0.721
4	1.0663	0.907	1.0063	0.867	0.8207	0.723
5	1.0787	0.910	1.0177	0.869	0.8296	0.724

$$\frac{d\dot{S}_{gen}}{\dot{m}c_p} = \frac{dx}{x + T_i/T^*} + \frac{P^*}{\rho c_p T^*}\frac{dx}{x + T_i/T^*} - \frac{q_w C\,dx}{\dot{m}c_p T_w}. \quad (31)$$

As the wall temperature is not explicitly defined in terms of the known variables, one replaces it by the dimensionless variable counterpart $\theta_w = (T_w - T_i)/(q_w a/k_e)$ where, in terms of the tabulated data, one has

$$T_w = T_i + (\theta_{1w} + Br\Phi_{1w})q_w a/k_e \quad (32)$$

leading to

$$\frac{d\dot{S}_{gen}}{\dot{m}c_p} = \frac{dx}{x + T_i/T^*} + F\frac{dx}{x + T_i/T^*} - \frac{q''C}{\dot{m}c_p T_i}\frac{dx}{1 + (\theta_{1w} + Br\Phi_{1w})q^*} \quad (33)$$

with the dimensionless wall heat flux being defined as $q^* = q_w a/(k_e T_i)$. Moreover, the dimensionless parameter $F = P^*/(\rho c_p T^*)$ is a measure of required pumping power to enthalpy change (longitudinal heat transfer). For non-zero Br values and in terms of the Darcy pressure drop one concludes that

$$F = N^*\frac{Br}{MDa}\Big/\left(\frac{4a}{D_H} + BrS^*\right), \quad (34)$$

where N^* shows the degree of non-Darcy effects on the longitudinal pressure gradient as $N^* = P^*/(\mu U/K)$. For the Darcy flow model $N^* = 1$. Integrating from $x = 0$ to $x = L$ and rearranging in terms of known parameters, one has

$$N_s = \frac{\dot{S}_{gen}(L)}{\dot{m}c_p}\ln\left[1 + q^*\widehat{L}\left(\frac{4a}{D_h} + BrS^*\right)\right]^{1+F} - q^*\frac{4a}{D_h}\int_0^{\widehat{L}}\frac{d\hat{x}}{1 + (\theta_{1w} + Br\Phi_{1w})q^*}. \quad (35a)$$

As seen, like the left-hand side term the first two terms in the right-hand side of Eq. (33) are integrated directly; however, the last term on the right side should be evaluated numerically. Before reporting the numerical results, which are obtained using the trapezoidal rule, two limiting cases, for which approximate closed form solutions are obtained, will be presented. It is assumed that the dimensionless heat flux q^* is very small compared to unity. Commensurate with that is the constant property assumption similar to [29]. First consider the case of a hyperporous medium for which one has $MDa = O(1)$. A quick check of Table 1 shows that for this case $S^* = O(1)$ so that neglecting the terms smaller that $O(q^*)$, like q^{*2}, one finds that

$$N_s = q^*\widehat{L}[F(1 + \bar{b})/\bar{b} + BrS^*(1 + F)]. \quad (35b)$$

Replacing F, one has

$$N_s = q^*\widehat{L}Br[S^* + N/(MDa)]. \quad (35c)$$

Table 4b
The difference between the dimensionless wall temperature and bulk temperature due to the wall effect and frictional heating contribution when $b/a = 4$

$\hat{x}$	$MDa = 1/100$		$MDa = 1/1000$		$MDa = 1/10{,}000$	
	$\theta_{1,w} - \theta_{1,b}$	$\Phi_{2,w} - \Phi_{2,b}$	$\theta_{1,w} - \theta_{1,b}$	$\Phi_{2,w} - \Phi_{2,b}$	$\theta_{1,w} - \theta_{1,b}$	$\Phi_{2,w} - \Phi_{2,b}$
0.0005	0.0575	0.113	0.0434	0.225	0.0344	0.328
0.0006	0.0610	0.124	0.0462	0.237	0.0368	0.337
0.0008	0.0673	0.143	0.0508	0.257	0.0410	0.352
0.001	0.0728	0.160	0.0549	0.273	0.0447	0.363
0.002	0.0941	0.218	0.0709	0.326	0.0593	0.393
0.003	0.1095	0.254	0.0831	0.356	0.0705	0.405
0.004	0.122	0.281	0.0931	0.377	0.0798	0.412
0.005	0.1324	0.301	0.1017	0.391	0.0877	0.416
0.006	0.1415	0.318	0.1093	0.402	0.0948	0.419
0.008	0.1569	0.344	0.1223	0.418	0.1069	0.423
0.01	0.1697	0.364	0.1333	0.428	0.1173	0.426
0.02	0.2155	0.423	0.1732	0.452	0.1556	0.433
0.03	0.2473	0.454	0.2012	0.462	0.1831	0.437
0.04	0.2721	0.474	0.2235	0.468	0.2050	0.438
0.05	0.2926	0.489	0.2420	0.473	0.2232	0.440
0.06	0.3100	0.500	0.2579	0.476	0.2389	0.440
0.08	0.3384	0.515	0.2842	0.480	0.2649	0.442
0.1	0.3609	0.527	0.3052	0.483	0.2857	0.442
0.2	0.4287	0.553	0.3692	0.491	0.3493	0.444
0.3	0.4628	0.563	0.4014	0.494	0.3814	0.445
0.4	0.4842	0.567	0.4212	0.495	0.4011	0.445
0.5	0.4999	0.569	0.4356	0.495	0.4152	0.445
0.6	0.5126	0.570	0.4471	0.495	0.4264	0.445
0.8	0.5332	0.571	0.4655	0.496	0.4443	0.445
1	0.5497	0.572	0.4802	0.496	0.4586	0.445
2	0.6010	0.573	0.5263	0.497	0.5035	0.445
3	0.6266	0.574	0.5495	0.497	0.5261	0.444
4	0.6401	0.575	0.5618	0.497	0.5381	0.444
5	0.6473	0.575	0.5684	0.497	0.5446	0.444

Comparing the predictions of the above equation and the numerically obtained results, a good degree of agreement is observed. For example with $b/a = 1$, $N^* = 0.1$, and $MDa = 1$, Eq. (35c) predicts $N_s = 0.4291$ and 0.0429 while the numerical results are 0.3435 and 0.0418 for $q^* = 0.01$ and 0.001, respectively. The results agree better for smaller q^* values, as expected based on our asymptotic analysis assumptions.

It is instructive to rearrange Eq. (35c) in terms of dimensional variables as

$$\dot{S}_{gen} = AL\frac{\mu_e U^2}{a^2 T_i}\left(S^* + \frac{N}{MDa}\right). \tag{35d}$$

Based on the Table 1 results, S^* decreases with the aspect ratio so that, as shown by Eq. (35d), the square cross-section is associated with the highest entropy generation rate compared to rectangular counterparts.

Another case of interest is the one for which $MDa \to 0$ where even for relatively small q^* one can still expect that the product of Brq^*S^* will be notably greater than O(1) so that the second term in the right side of Eq. (35a) is negligible compared to the first one; a term that can be simplified in such a way that N_s be obtained as

$$N_s = \left(1 + \frac{N}{MDaS^*}\right)\ln\left(\frac{\mu_e U}{\rho c_p T_i a}\frac{L}{a}S^*\right) \tag{35e}$$

similar to the previous case, Eq. (35e) has been verified versus numerical counterparts for $MDa = 10^{-4}$ and $N^* = 1$ with the other parameters remaining the same. The numerical results are $N_s = 12.249$, 7.814 while approximate counterparts are 12.344 and 7.785 for $q^* = 0.01$ and 0.001, respectively.

3. Results and discussion

In the absence of frictional heating contribution, under the constant wall heat flux condition, the energy balance leads to a relation for the bulk temperature,

$$\theta_{1,b} = (1 + \bar{b})\hat{x}/\bar{b}. \tag{36a}$$

The bulk temperature is also obtainable analytically with $\theta(\bar{y}, \bar{z}; \hat{x})$ from Eq. (16). This was done mainly for the verification of the mathematical relations for the temperature solution. Similarly, the application of energy balance to a material element yields the relation

$$\Phi_{2,b} = S^*\hat{x} \tag{36b}$$

and S^* values for selected values of b/a and MDa values are in Table 1.

If one designates $\theta_w = (T_w - T_i)/(q_w a/k_e)$ and $\theta_b = (T_b - T_i)/(q_w a/k_e)$, the Nusselt number is obtainable from the relation $Nu = ha/k_e = 1/(\theta_w - \theta_b)$ and then using the

Table 5a
The difference between the dimensionless wall temperature and bulk temperature due to the wall effect and frictional heating contribution when $b/a = 10$

$\hat{x}$	$MDa = \infty$		$MDa = 1$		$MDa = 1/10$	
	$\theta_{1,w} - \theta_{1,b}$	$\Phi_{2,w} - \Phi_{2,b}$	$\theta_{1,w} - \theta_{1,b}$	$\Phi_{2,w} - \Phi_{2,b}$	$\theta_{1,w} - \theta_{1,b}$	$\Phi_{2,w} - \Phi_{2,b}$
0.0005	0.0893	0.028	0.0878	0.035	0.0779	0.050
0.0006	0.0947	0.032	0.0930	0.039	0.0824	0.055
0.0008	0.1041	0.039	0.1020	0.047	0.0902	0.065
0.001	0.1122	0.045	0.1096	0.054	0.0969	0.074
0.002	0.1420	0.072	0.1379	0.083	0.1215	0.109
0.003	0.1633	0.094	0.1582	0.106	0.1391	0.135
0.004	0.1803	0.115	0.1745	0.125	0.1533	0.157
0.005	0.1948	0.134	0.1883	0.143	0.1654	0.176
0.006	0.2074	0.151	0.2004	0.158	0.1759	0.193
0.008	0.2287	0.182	0.2211	0.186	0.1941	0.221
0.01	0.2465	0.210	0.2385	0.211	0.2094	0.246
0.02	0.3087	0.311	0.2999	0.303	0.2643	0.332
0.03	0.3498	0.379	0.3407	0.369	0.3012	0.388
0.04	0.3809	0.431	0.3713	0.420	0.3291	0.429
0.05	0.4061	0.473	0.3960	0.462	0.3515	0.462
0.06	0.4272	0.509	0.4166	0.498	0.3702	0.488
0.08	0.4612	0.565	0.4495	0.555	0.4000	0.529
0.1	0.4877	0.609	0.4751	0.598	0.4229	0.560
0.2	0.5651	0.725	0.5492	0.709	0.4880	0.638
0.3	0.6039	0.765	0.5853	0.746	0.5176	0.664
0.4	0.6292	0.781	0.6084	0.761	0.5351	0.673
0.5	0.6490	0.788	0.6262	0.767	0.5479	0.677
0.6	0.6658	0.792	0.6412	0.771	0.5584	0.679
0.8	0.6944	0.798	0.6666	0.775	0.5761	0.682
1	0.7188	0.801	0.6882	0.778	0.5911	0.683
2	0.8082	0.811	0.7673	0.786	0.6459	0.686
3	0.8703	0.815	0.8223	0.790	0.6841	0.688
4	0.9185	0.818	0.8649	0.792	0.7139	0.689
5	0.9579	0.820	0.8997	0.794	0.7383	0.689

hydraulic diameter $D_h = 4ab/(a+b)$ in the definition, the Nusselt number becomes

$$Nu_D = \frac{D_h}{a}Nu = \frac{4\bar{b}}{1+\bar{b}}\left(\frac{1}{\theta_w - \theta_b}\right) = \frac{4\bar{b}}{1+\bar{b}}\left[\frac{1}{(\theta_{1,w}-\theta_{1,b}) + Br(\Phi_{2,w}-\Phi_{2,b})}\right]. \quad (37)$$

The values of Nu_D can be determined from tabulated $(\theta_{1,w}-\theta_{1,b})$ and $(\Phi_{2,w}-\Phi_{2,b})$ data in Tables 2a,b to 5a,b, at different $\hat{x} = (x/a)/Pe$, b/a, MDa, and Br values which can be positive or negative depending on the direction of heat flux.

The data for $\Phi_{2,w}-\Phi_{2,b}$ can also identify the values of the wall temperature in the absence of heating or cooling at the walls where viscous dissipation is the only reason for heat transfer as discussed by Hooman et al. [24] for a similar problem with isothermal wall heating. In this case the energy generated inside the duct should be carried by the moving fluid leading to an increase in the fluid enthalpy. For this case one obtains the wall and bulk temperature as

$$\frac{T_w(y,z;x) - T_i}{\mu_e U^2/k_e} = \Phi_{2,w}(\bar{y},\bar{z};\hat{x}), \quad (38a)$$

$$\frac{T_b(y,z;x) - T_i}{\mu_e U^2/k_e} = \Phi_{2,b}(\bar{y},\bar{z};\hat{x}) = S^*\hat{x}. \quad (38b)$$

One notes that the temperature scale is $\mu_e U^2/k_e$ for this case as there is no wall heat flux to be included in the denominator. The data in Tables 2a,b to 5a,b can be used to illustrate the wall–bulk temperature difference $\Phi_{2,w}-\Phi_{2,b}$. This has been done for some cases as shown in Fig. 2a–d for $b/a = 1$, 2, 4, and 10 where the variations of the wall temperature $\theta_{1,w}$ and the bulk temperature $\theta_{1,b}$ are graphically presented in [21] for the same aspect ratios. As a common trend in all charts on Fig. 2a–d, one observes that $\Phi_{2,w}-\Phi_{2,b}$ increases along the duct. However, with $MDa > 0.1$ the curve experiences a turning point while for smaller values of MDa there is a sharp increase in $\Phi_{2,w}-\Phi_{2,b}$.

For a more comprehensive analysis of the problem, one can use the data presented in Tables 1–5 to find the Nusselt number for any arbitrary combination of the key parameters. As an illustration, this is partly done and the results are in Figs. 3 and 4. Fig. 3a shows the developing Nusselt number for $MDa = 0.001$ versus $\hat{x}$ for several values of Br. It is clear that increasing Br will reduce the Nusselt number level. Moreover, increasing Br and aspect ratio, the Nu_D versus $\hat{x}$ plots tend to be more flattened. The square cross-section seems to behave differently for higher Br values in such a way that the developing Nusselt number is as high as that of other aspect ratios in the duct entrance and then decreases sharply with the fully developed Nu_D being the minimum among the other counterparts. It is interest-

Table 5b
The difference between the dimensionless wall temperature and bulk temperature due to the wall effect and frictional heating contribution when $b/a = 10$

$\hat{x}$	$MDa = 1/100$		$MDa = 1/1000$		$MDa = 1/10{,}000$	
	$\theta_{1,w}-\theta_{1,b}$	$\Phi_{2,w}-\Phi_{2,b}$	$\theta_{1,w}-\theta_{1,b}$	$\Phi_{2,w}-\Phi_{2,b}$	$\theta_{1,w}-\theta_{1,b}$	$\Phi_{2,w}-\Phi_{2,b}$
0.0005	0.0594	0.112	0.0455	0.244	0.0371	0.313
0.0006	0.0628	0.122	0.0481	0.256	0.0394	0.325
0.0008	0.0689	0.140	0.0527	0.275	0.0434	0.341
0.001	0.0740	0.154	0.0567	0.290	0.0469	0.353
0.002	0.0932	0.206	0.0720	0.335	0.0605	0.378
0.003	0.1070	0.239	0.0832	0.360	0.0709	0.387
0.004	0.1182	0.265	0.0925	0.376	0.0796	0.392
0.005	0.1277	0.285	0.1005	0.387	0.0872	0.396
0.006	0.1361	0.302	0.1076	0.396	0.0940	0.399
0.008	0.1506	0.329	0.1200	0.409	0.1059	0.402
0.01	0.1629	0.350	0.1307	0.418	0.1162	0.405
0.02	0.2076	0.413	0.1703	0.443	0.1549	0.411
0.03	0.2381	0.445	0.1980	0.455	0.1823	0.413
0.04	0.2614	0.466	0.2197	0.463	0.2038	0.414
0.05	0.2803	0.480	0.2374	0.468	0.2215	0.414
0.06	0.2962	0.491	0.2524	0.471	0.2365	0.414
0.08	0.3219	0.506	0.2769	0.476	0.2609	0.414
0.1	0.3418	0.517	0.2961	0.479	0.2802	0.415
0.2	0.3990	0.543	0.3521	0.487	0.3367	0.415
0.3	0.4245	0.552	0.3774	0.489	0.3624	0.415
0.4	0.4388	0.555	0.3914	0.490	0.3766	0.415
0.5	0.4486	0.556	0.4007	0.491	0.3860	0.415
0.6	0.4564	0.557	0.4080	0.491	0.3932	0.415
0.8	0.4693	0.558	0.4198	0.491	0.4049	0.415
1	0.4803	0.558	0.4297	0.491	0.4147	0.415
2	0.5205	0.559	0.4661	0.491	0.4507	0.415
3	0.5487	0.559	0.4918	0.492	0.4761	0.415
4	0.5708	0.559	0.5118	0.492	0.4959	0.415
5	0.5889	0.559	0.5283	0.492	0.5122	0.415

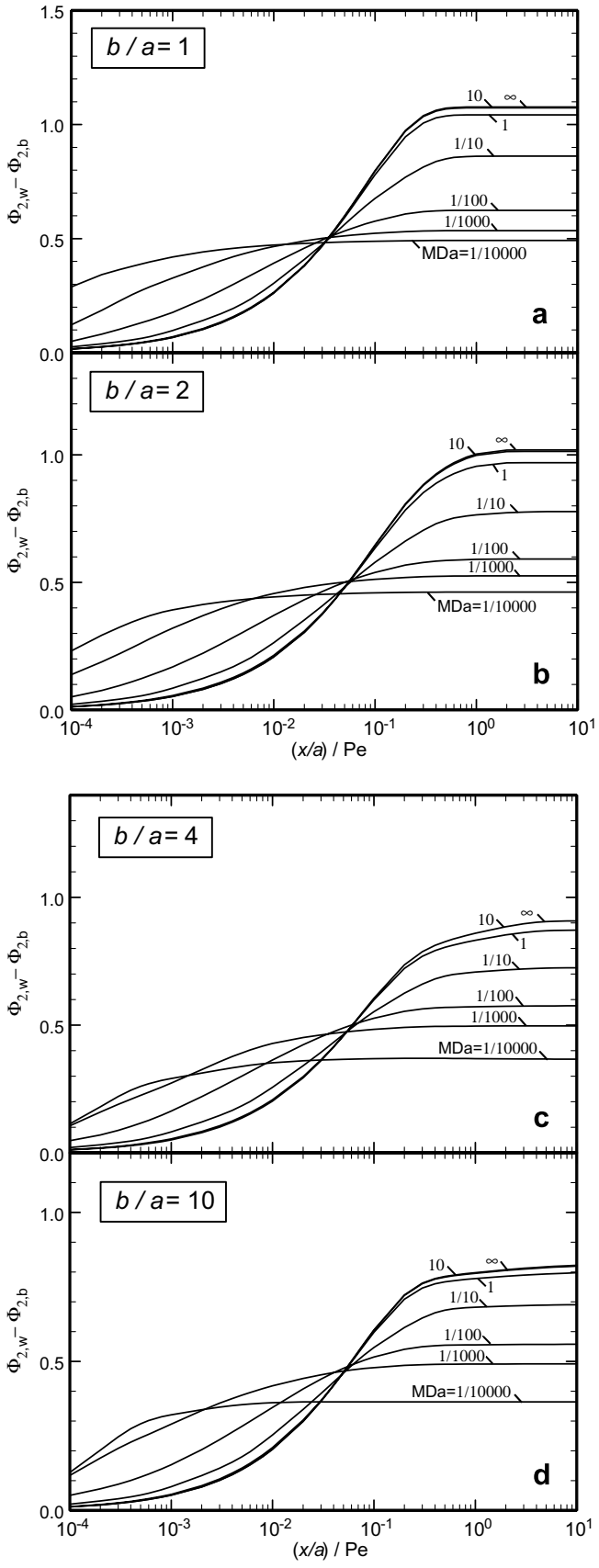

Fig. 2. The effects of frictional heating on the wall–bulk temperature difference for different *MDa* values in the absence of wall heat flux, when (a) $b/a = 1$, (b) $b/a = 2$, (c) $b/a = 4$, and (d) $b/a = 10$.

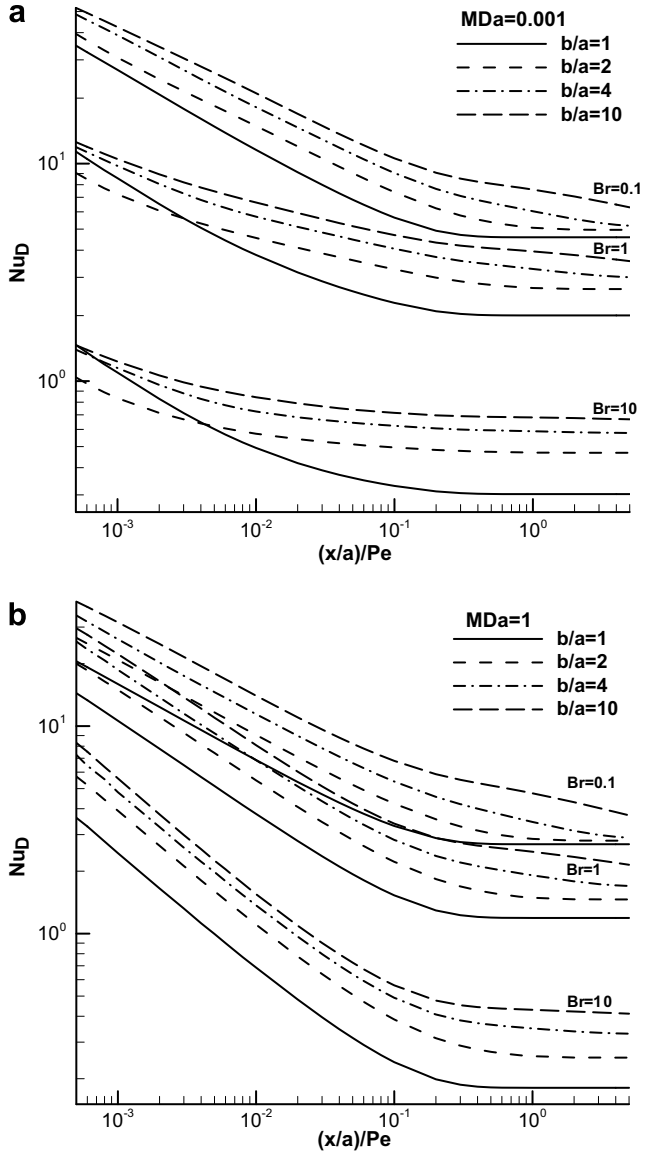

Fig. 3. Nu_D versus $(x/a)/Pe$ for different *Br* and aspect ratio values, (a) when $MDa = 0.001$ and (b) when $MDa = 1$.

ing that in their study of heat transfer and entropy generation in a duct of rectangular cross-section with the fully developed assumption, Hooman et al. [29] have reported that the square cross-section acts in a different manner for very small *MDa* values where the velocity profile is nearly slug and the problem is a conduction-like one. They attributed this fact (in part) to the special geometry of a square for having more symmetry compared to rectangular counterparts. Fig. 3b shows Nu_D versus longitudinal coordinate for different *Br* values with $MDa = 1$ which represents a hyperporous medium. It can be concluded that for a fixed *Br* value Nu_D increases with the aspect ratio for all cases considered here.

Fig. 4a and b presents the fully developed Nu_D versus *Br* for two limiting aspect ratios being $b/a = 1$ and 10. One realizes that the hyperporous case, with $MDa = 1$, mimics

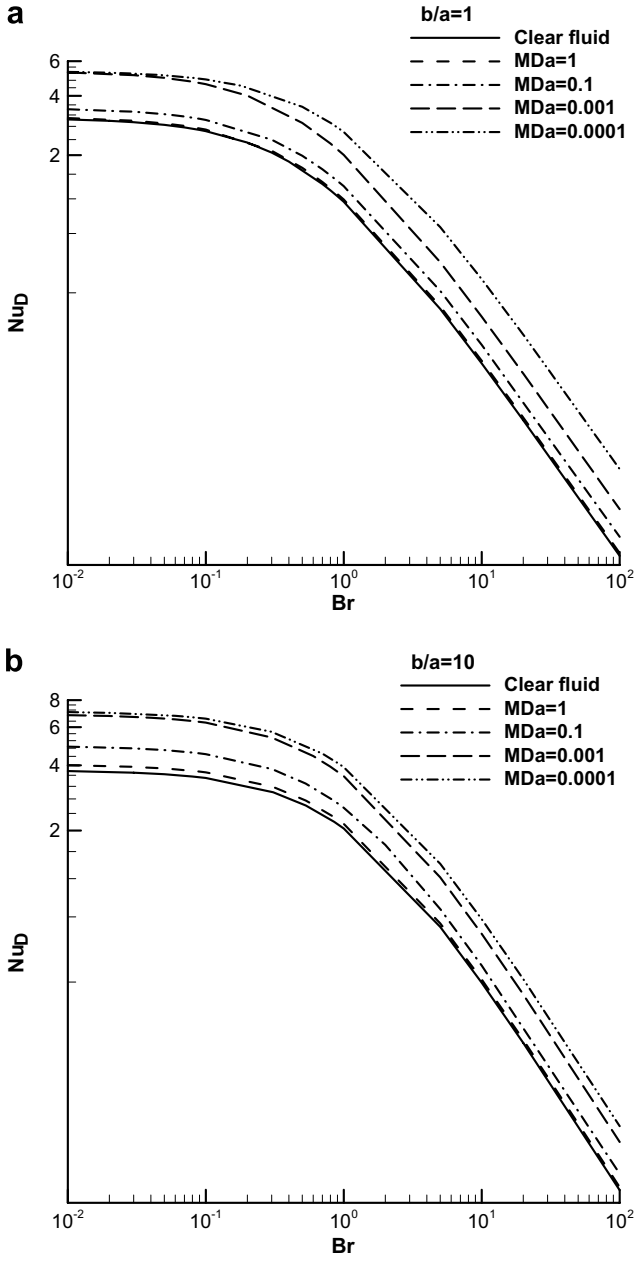

Fig. 4. Fully developed Nu_D versus Br, MDa, and aspect ratio values, (a) when $b/a = 1$ and (b) when $b/a = 10$.

the clear fluid counterpart as the corresponding curves are nearly identical but moving from $MDa = 0.0001$ to 0.001, changes in the Nusselt number are more pronounced compared to the former case. In line with the aforementioned observations increasing Br or decreasing MDa will decrease the Nusselt number for either values of the duct aspect ratio. Moreover, the Nusselt number puts higher values for smaller aspect ratio compared to the higher one. Nevertheless, it should be noted that, for small Br values, selection of a length scale in the Nusselt number (hydraulic diameter) is partly responsible for that similar to what was reported by [29]. Interestingly, moving to higher Br values, this choice becomes of less importance.

For a better understanding of the problem, Eq. (37) is rearranged in terms of the Nusselt number for negligible viscous dissipation case, Nu^*, as follows

$$Nu_{\mathrm{D}} = \frac{4\bar{b}}{1+\bar{b}}\left[\frac{1}{Nu^*} + Br(\Phi_{2,\mathrm{w}} - \Phi_{2,\mathrm{b}})\right]^{-1}. \tag{39}$$

Eq. (39) is identical to the form reported by Kakaç et al. [33] for clear flow through a pipe and also by Hooman and Gurgenci [34] for a parallel plate porous channel (see [35–37] for more closed form solutions for similar problems), if rearranged as follows

$$Nu_{\mathrm{D}} = \frac{4\bar{b}}{1+\bar{b}}\left[\frac{Nu^*}{1 + Nu^* Br(\Phi_{2,\mathrm{w}} - \Phi_{2,\mathrm{b}})}\right]. \tag{40}$$

It is an easy task to see that increasing Br decreases Nu_{D} where Nu^* is the Nusselt number for the case where one can neglect the viscous dissipation effects. Eq. (40) can be modified to be used for ducts of other cross-sections. The significance of this point becomes more vivid as one can apply Eq. (40) to account for the viscous dissipation effects, for the fully developed or thermally developing region, by combining two easier problems, with their answers available in the literature, to obtain the solution to a more complex problem. For example one can use the correlations proposed by Haji-Sheikh [38] to find Nu^* for parallel plate channels or circular tubes and solve only for the second part to obtain the final solution for a problem where frictional heating is important. This seems to be of practical importance in engineering applications where usually one is in search for a rough and ready estimate rather than complicated calculations.

It is worth noting that several combinations of the key parameters can lead to different results, based on the data in Tables 2–5; however, for the sake of brevity, we restrict our results for the second law aspects of the problem to the

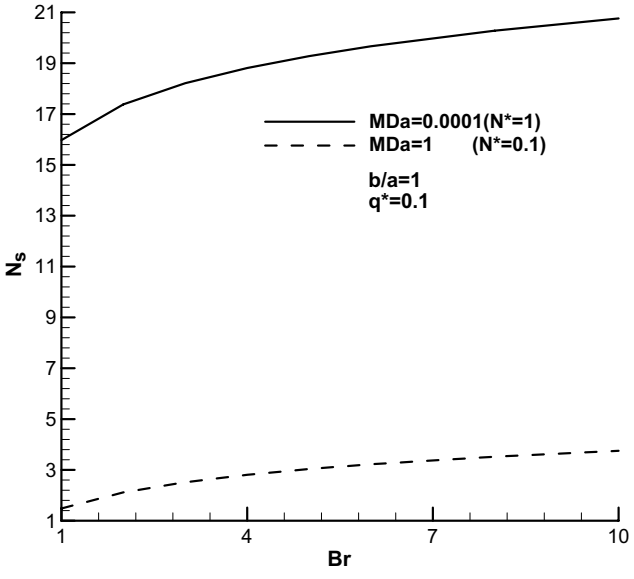

Fig. 5. Variation of N_s versus Br for different values of MDa.

most irreversible geometry being the square cross-section (see [11–13,29]). Fig. 5 illustrates plots of N_s versus Br for two different values of MDa being 1 and 10^{-4}. As seen, with the other parameters fixed, decreasing MDa or increasing either of Br or q^* increases the entropy production rate. This is in line with the results of Hooman et al. [29]. Moving from $MDa = 1$ to 10^{-4}, the N_s–Br slope changes as expected based on the approximate predictions of Eqs. (35d) and (35e).

4. Conclusion

The effect of viscous dissipation on heat transfer and entropy generation for thermally developing forced convection in a porous-saturated duct of rectangular cross-section is investigated. The classical Galerkin method is applied to solve the Brinkman momentum equation while the EWRM is undertaken to solve the non-homogenous three-dimensional thermal energy equation. It is believed that the solution reported in this study can serve as a benchmark for verification of numerical solutions concerning similar problems for example those addressed by [39–46]. It was observed that viscous dissipation reduces the Nusselt number in both thermally developing and fully developed regions unlike the similar case with isothermal wall heating. Key parameters affecting the second law aspects of the problem are highlighted and analyzed.

Acknowledgement

The first author, the scholarship holder, acknowledges the financial support provided by The University of Queensland in terms of UQILAS, Endeavor IPRS, and School scholarship.

References

[1] D.A. Nield, A. Bejan, Convection in Porous Media, third ed., Springer, New York, 2006.
[2] H.I. Ene, E. Sanchez-Palencia, On thermal equation for flow in porous media, Int. J. Eng. Sci. 20 (1982) 623–630.
[3] D.A. Nield, Resolution of a paradox involving viscous dissipation and nonlinear drag in a porous medium, Trans. Porous Media 41 (2000) 349–357.
[4] A.K. Al-Hadhrami, L. Elliot, D.B. Ingham, A new model for viscous dissipation in porous media across a range of permeability values, Trans. Porous Media 53 (2003) 117–122.
[5] W.P. Breugem, D.A.S. Rees, A derivation of the volume-averaged Boussinesq equations for flow in porous media with viscous dissipation, Trans. Porous Media 63 (2006) 1–12.
[6] D.A. Nield, Modelling fluid flow in saturated porous media and at interfaces, in: D.B. Ingham, I. Pop (Eds.), Transport Phenomena in Porous Media II, Elsevier Science, Oxford, 2002.
[7] D.A. Nield, A note on a Brinkman–Brinkman forced convection problem, Trans. Porous Media 64 (2006) 185–188.
[8] D. Bercovici, Generation of plate tectonics from lithosphere-mantle flow and void-volatile self-lubrication, Earth Planet. Sci. Lett. 154 (1998) 139–151.
[9] G.P. Celata, G.L. Morini, V. Marconi, S.J. McPhail, G. Zummo, Using viscous heating to determine the friction factor in microchannels – an experimental validation, Exp. Therm. Fluid Sci. 30 (2006) 725–731.
[10] Y. Murakami, B. Mikic, Parametric investigation of viscous dissipation effects on optimized air cooling microchanneled heat sinks, Heat Transfer Eng. 24 (2003) 53–62.
[11] A. Bejan, Entropy Generation through Heat and Fluid Flow, Wiley, New York, 1982.
[12] A.Z. Sahin, Irreversibilities in various duct geometries with constant wall heat flux and laminar flow, Energy 23 (1998) 465–473.
[13] E.B. Ratts, A.G. Raut, Entropy generation minimization of fully developed internal flow with constant heat flux, ASME J. Heat Transfer 126 (2004) 656–659.
[14] A.C. Baytas, Entropy generation for free and forced convection in a porous cavity and a porous channel, in: D.B. Ingham et al. (Eds.), Emerging Technology and Techniques in Porous Media, Kluwer Academic Publishers, 2004, pp. 259–270.
[15] K. Hooman, A. Ejlali, Entropy generation for forced convection in a porous saturated circular tube with uniform wall temperature, Int. Commun. Heat Mass Transfer 34 (2007) 408–419.
[16] K. Hooman, Entropy-energy analysis of forced convection in a porous-saturated circular tube considering temperature-dependent viscosity effects, Int. J. Exergy 3 (2006) 436–451.
[17] K. Hooman, A. Ejlali, Second law analysis of laminar flow in a channel filled with saturated porous media: a numerical solution, Entropy 7 (2005) 300–307.
[18] A. Haji-Sheikh, K. Vafai, Analysis of flow and heat transfer in porous media imbedded inside various-shaped ducts, Int. J. Heat Mass Transfer 47 (2004) 1889–1905.
[19] A. Haji-Sheikh, Fully developed heat transfer to fluid flow in rectangular passages with filled with porous materials, ASME J. Heat Transfer 128 (2006) 822–828.
[20] A. Haji-Sheikh, W.J. Minkowycz, E.M. Sparrow, Green's function solution of temperature field for flow in porous passages, Int. J. Heat Mass Transfer 47 (2004) 4685–4695.
[21] A. Haji-Sheikh, D.A. Nield, K. Hooman, Heat transfer in thermal entrance region for flow through rectangular porous passages, Int. J. Heat Mass Transfer 49 (2006) 3004–3015.
[22] A. Haji-Sheikh, W.J. Minkowycz, E.M. Sparrow, A numerical study of the heat transfer to fluid flow through circular porous passages, Numer. Heat Transfer A 46 (2004) 929–955.
[23] A. Haji-Sheikh, E.M. Sparrow, W.J. Minkowycz, Heat transfer to flow through porous passages using extended weighted residuals method—a Green's function solution, Int. J. Heat Mass Transfer 48 (2005) 1330–1349.
[24] K. Hooman, A. Haji-Sheikh, D.A. Nield, Thermally developing Brinkman–Brinkman forced convection in rectangular ducts with isothermal walls, Int. J. Heat Mass Transfer, in press, doi:10.1016/j.ijheatmasstransfer.2007.01.011.
[25] K. Hooman, A.A. Merrikh, Analytical solution of forced convection in a duct of rectangular cross-section saturated by a porous medium, ASME J. Heat Transfer 128 (2006) 596–600.
[26] K. Hooman, H. Gurgenci, Effects of temperature-dependent viscosity variation on entropy generation, heat, and fluid flow through a porous-saturated duct of rectangular cross-section, Appl. Math. Mech. – Engl. ed. 28 (2007) 69–78.
[27] K. Hooman, Fully developed temperature distribution in porous saturated duct of elliptical cross-section, with viscous dissipation effects and entropy generation analysis, Heat Transfer Res. 36 (2005) 237–245.
[28] K. Hooman, Analysis of entropy generation in porous media imbedded inside elliptical passages, Int. J. Heat Technol. 23 (2005) 145–149.
[29] K. Hooman, H. Gurgenci, A.A. Merrikh, Heat transfer and entropy generation optimization of forced convection in a porous-saturated duct of rectangular cross-section, Int. J. Heat Mass Transfer 50 (2007) 2051–2059.
[30] R.K. Shah, A.L. London, Laminar flow forced convection in ducts, Advances in Heat Transfer, Academic Press, New York, 1978, Suppl. 1.

[31] L.V. Kantorovich, V.I. Krylov, Approximate Methods of Higher Analysis, Wiley, New York, 1960.
[32] J.V. Beck, K. Cole, A. Haji-Sheikh, B. Litkouhi, Heat Conduction Using Green's Functions, Hemisphere Publ. Corp., Washington D.C., 1992.
[33] S. Kakaç, R.K. Shah, W. Aung, Handbook of Single-Phase Convective Heat Transfer, Wiley, New York, 1987.
[34] K. Hooman, H. Gurgenci, Effects of viscous dissipation and boundary conditions on forced convection in a channel occupied by a saturated porous medium, Trans. Porous Media (2007), doi:10.1007/s11242-006-9049-4.
[35] D.A. Nield, A.V. Kuznetsov, M. Xiong, Effects of viscous dissipation and flow work on forced convection in a channel filled by a saturated porous medium, Trans. Porous Media 56 (2004) 351–367.
[36] D.A. Nield, K. Hooman, Comments on ''Effects of viscous dissipation on the heat transfer in forced pipe flow. Part 1: both hydrodynamically and thermally fully developed flow, and Part 2: thermally developing flow" by O. Aydin, Energy Conv. Manag. 47 (2006) 3501–3503.
[37] K. Hooman, A. Pourshaghaghy, A. Ejlali, Effects of viscous dissipation on thermally developing forced convection in a porous saturated circular tube with an isoflux wall, Appl. Math. Mech. 27 (2006) 617–626.
[38] A. Haji-Sheikh, Estimation of average and local heat transfer in parallel plates and circular ducts filled with porous materials, ASME J. Heat Transfer 126 (2004) 400–409.
[39] A.R.A. Khaled, K. Vafai, Analysis of flow heat transfer inside nonisothermal squeezed thin films, Numer. Heat Transfer A 47 (10) (2005) 981–996.
[40] S.V. Iyer, K. Vafai, Passive heat transfer augmentation in a cylindrical annulus utilizing a porous perturbation, Numer. Heat Transfer A 36 (2) (1999) 115–128.
[41] S.S. Mousavi, K. Hooman, Heat fluid flow in entrance region of a channel with staggered baffles, Energy Convers. Manage. 47 (15–16) (2006) 2011–2019.
[42] K. Khanafer, K. Vafai, Double-diffusive mixed convection in a lid-driven enclosure filled with a fluid-saturated porous medium, Numer. Heat Transfer A 42 (5) (2002) 465–486.
[43] K. Hooman, A perturbation solution for forced convection in a porous-saturated duct, J. Comput. Appl. Math. (2006), doi:10.1016/j.cam.2006.11.005.
[44] A. Narasimhan, J.L. Lage, Forced convection of a fluid with temperature-dependent viscosity flowing through a porous medium channel, Numer. Heat Transfer A 40 (2001) 801–820.
[45] S.C. Chen, K. Vafai, Non-Darcian surface tension effects on free surface transport in porous media, Numer. Heat Transfer A 31 (1997) 235–254.
[46] P.C. Huang, K. Vafai, Internal heat transfer augmentation in a channel using an alternate set of porous cavity-block obstacles, Numer. Heat Transfer A 25 (1994) 519–539.